Design and installation of a ferromagnetic wall in tokamak geometry

P. E. Hughes, J. P. Levesque, N. Rivera, M. E. Mauel, and G. A. Navratil

Citation: Review of Scientific Instruments **86**, 103504 (2015); doi: 10.1063/1.4932312
View online: https://doi.org/10.1063/1.4932312
View Table of Contents: http://aip.scitation.org/toc/rsi/86/10
Published by the American Institute of Physics

Articles you may be interested in

Active and passive kink mode studies in a tokamak with a movable ferromagnetic wall
Physics of Plasmas **22**, 056102 (2015); 10.1063/1.4918360

Discovery of stationary operation of quiescent H-mode plasmas with net-zero neutral beam injection torque and high energy confinement on DIII-D
Physics of Plasmas **23**, 056103 (2016); 10.1063/1.4943521

Equilibrium reconstruction with 3D eddy currents in the Lithium Tokamak eXperiment
Physics of Plasmas **24**, 042513 (2017); 10.1063/1.4981214

Rotational stabilization of the resistive wall modes in tokamaks with a ferritic wall
Physics of Plasmas **22**, 032509 (2015); 10.1063/1.4915129

Magnetic perturbation diagnostics in the high-temperature lithiated environment of LTX-β
Review of Scientific Instruments **89**, 10J104 (2018); 10.1063/1.5035359

Turbulent fluctuations during pellet injection into a dipole confined plasma torus
Physics of Plasmas **24**, 012506 (2017); 10.1063/1.4973828

PHYSICS TODAY
WHITEPAPERS
MANAGER'S GUIDE
Accelerate R&D with Multiphysics Simulation
READ NOW
PRESENTED BY
COMSOL

Design and installation of a ferromagnetic wall in tokamak geometry

P. E. Hughes,[a] J. P. Levesque, N. Rivera, M. E. Mauel, and G. A. Navratil
Columbia University Plasma Physics Laboratory, Columbia University, 102 S.W. Mudd, 500 W. 120th St., New York, New York 10027, USA

(Received 30 March 2015; accepted 22 September 2015; published online 8 October 2015)

Low-activation ferritic steels are leading material candidates for use in next-generation fusion development experiments such as a prospective component test facility and DEMO power reactor. Understanding the interaction of plasmas with a ferromagnetic wall will provide crucial physics for these facilities. In order to study ferromagnetic effects in toroidal geometry, a ferritic wall upgrade was designed and installed in the High Beta Tokamak–Extended Pulse (HBT-EP). Several material options were investigated based on conductivity, magnetic permeability, vacuum compatibility, and other criteria, and the material of choice (high-cobalt steel) is characterized. Installation was accomplished quickly, with minimal impact on existing diagnostics and overall machine performance, and initial results demonstrate the effects of the ferritic wall on plasma stability. © *2015 AIP Publishing LLC.* [http://dx.doi.org/10.1063/1.4932312]

I. INTRODUCTION

Current-generation magnetic confinement plasma devices make extensive use of austenitic stainless steels, particularly SAE 316, for their combination of material strength and weak response to applied magnetic fields. However, the high chromium, nickel, and molybdenum content in stainless steels makes them particularly vulnerable to damage and radioactivation from the very high fast neutron fluences expected in burning plasma devices.[1] Currently, the best material solution to this problem is the use of a family of low-activation ferritic steels engineered for resistance to neutron damage.[2] Additionally, tokamak fusion devices are expected to require ferritic inserts to reduce the toroidal field ripple non-axisymmetry introduced by the presence of discrete toroidal field magnets.[3] However, the ferromagnetic response of these materials is expected to amplify certain plasma instabilities. Because the ferromagnetic material's magnetic permeability is greater than that of vacuum, a ferritic wall soaks in magnetic energy from the vacuum bounding the plasma. This reduces the vacuum energy available to balance the potential energy of the plasma, making instabilities more serious and expanding the unstable parameter space to include the ferritic wall mode (FWM).[4,5]

To date, research into the effects of ferritic wall components on plasma stability in tokamak geometry has been oriented toward verifying the feasibility of machine operation in best-case scenarios, e.g., components with low magnetic permeability and long soak-through times,[3] although an experiment in cylindrical geometry observed enhanced instability under suitable conditions.[6] The High Beta Tokamak–Extended Pulse (HBT-EP) machine's radially adjustable, toroidally segmented stabilizing walls[7] make it especially well-suited to studying the effects of ferritic material on plasma stability by allowing the modular retraction of a toroidal subset of wall sections (Fig. 1), without breaching the vacuum vessel to change the wall configuration.

II. WALL UPGRADE DESIGN

While the ~5 T toroidal field of a reactor is expected to drive low-activation steels deep into magnetic saturation ($\mu_r \sim 2$),[8] the ferritic effect is expected to scale with fractional coverage and with wall thickness relative to plasma minor radius.[4] Given the reduced ferritic wall coverage in HBT-EP (~12% of the plasma surface), observing the ferritic wall mode in HBT-EP requires either a very thick wall ($d > 2$ cm in HBT-EP)[9] or a thinner wall with higher permeability.[3] To be compatible with standard HBT-EP discharges, it was necessary to select a ferritic material from a range of possibilities that would maintain a high relative magnetic permeability μ_r between 5 and 10 in HBT-EP's typical 3.3 kG toroidal magnetic field.[7] The three main categories of materials investigated were ferrite ceramics, work-hardened stainless steels, and specialty alloys developed for magnetic shielding applications. The primary physical characteristics of interest to us were high saturation induction, low conductivity, ultra-high vacuum (UHV) compatibility, and ease of fabrication.

Ferrite ceramics, sintered composite materials used in inductors, transformers, and RF chokes, are employed particularly for their extremely high resistivity, making them attractive for studies intending to compare against theory, as the reduction of effective μ by eddy currents is negligible. However, the saturation induction is generally of order 5 kG, much lower than the saturation induction in ferritic steels. Additionally, sintered materials in general have very poor vacuum compatibility at the nTorr range in which HBT-EP operates. Furthermore, the far greater resistivity would preclude studying the frequency-dependence of the ferritic effect due to eddy currents, effectively ignoring the finite wall thickness, suggested to be important in theoretical treatments.[5]

Certain stainless steels (especially SAE 304 and 301) can potentially be work-hardened to magnetic permeabilities of order 10 in modest applied fields.[10] Although they have finite conductivities, they are significantly lower than those of other metals and even most other steels. The reproducibility of magnetic properties due to work-hardening was deemed to be

[a]Electronic mail: peh2109@columbia.edu

 © 2015 AIP Publishing LLC

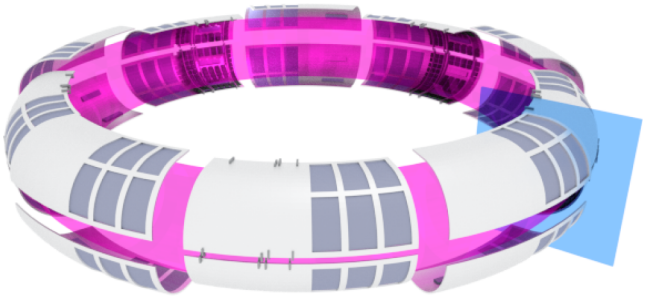

FIG. 1. Rendering of HBT-EP plasma with five stabilizing wall or "shell" pairs with ferritic segments fully inserted and five unmodified pairs fully retracted. Movable shells are light gray with dark gray control coil windows, and ferritic tiles are in black. The blue plane marks the poloidal cross section seen in Fig. 3(b), and transparent magenta represents the plasma.

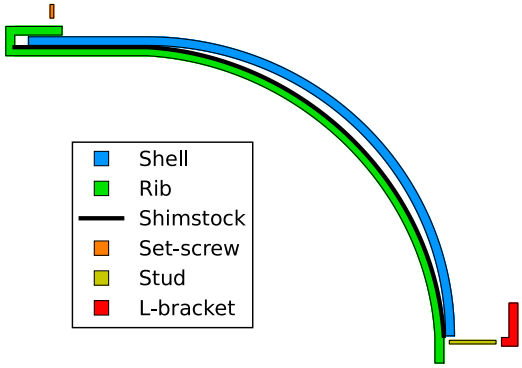

FIG. 2. Poloidal cross-section diagram of a poloidal rib of the mounting frame shown with the nominal shell and all mounting assembly parts. These include a setscrew at the back of the shell to secure the U-hook at the inboard edge, and the stud and custom L-bracket securing the rib at the midplane edge. The L-bracket was fastened on with a lock washer and nut not shown here.

too unreliable, however, and the exact procedure for achieving a target magnetic permeability would have required lengthy study and development.

There is a wide range of steels engineered especially for saturation inductions exceeding 2 T. They have conductivities in the range typical of steels and are commercially mass-produced materials, especially common as thin sheet for magnetic shielding due to the combination of the steel-like mechanical properties and very large values of μ_r at low applied fields.

For the ferritic wall upgrade, HBT-EP used Hiperco® 50 alloy, a high-cobalt iron alloy (detailed in ASTM 801a) from Carpenter Technology Corporation.[10] Hiperco 50 alloy has a manufacturer-listed saturation induction ($\mu_0 M_{sat}$) of over 2.4 T, with saturation beginning at about 800A/m (10 Oe) or less,[11] consistent with accepted values for similar alloys.[12] Because the strength of HBT-EP's equilibrium fields is much larger than required for saturation, the expected relative permeability is $\mu_r \approx 8$, as discussed in Section V. Its conductivity is relatively high, roughly twice that of 316 stainless steel, but it has none of the vacuum performance concerns of ferrite ceramics, and none of the problems with reproducibility and intensive customization of work-hardened stainless steel.

Because of the high conductivity of Hiperco 50 alloy and because the intention was to maximize the ferritic effects while moderating the effects of eddy currents, the ferritic wall segments were designed as a set of tiles. This approach not only reduced eddy currents, but also drastically simplified the construction of close-fitting, easily custom-fitted panels using a set of conformal poloidal ribs to grip the shell (Fig. 2). The tiles could be attached to these ribs by a flexible substrate. Thin stainless shim stock was flexible but strong enough to mount the tiles securely to the ribs, provided that short toroidal ribs were added to prevent the shim stock from buckling.

It should be noted that Hiperco 50 alloy cannot be electropolished due to its lack of chromium. Instead, the tiles were tumbled in a rock tumbler with coarse ceramic grit to smooth the sharp edges left by cutting and reduce the risk of arcing. However, the tiles developed a film of residue after tumbling. This residue was difficult and time-intensive to remove by scrubbing, but sandblasting proved faster and more effective. The tiles were also cleaned thoroughly in acetone and then methanol, as were all other parts to be installed in-vessel and all tools used for in-vessel work.

The tiled configuration simplified fabrication enough that it was possible to do most of the assembly on site, although the cutting of the tiles and the ribs was performed by a custom steel working company on a water jet table, and the TIG welding of the frames was performed by a custom welding company. The Hiperco 50 alloy tiles, each approximately 1 in.^{2} in surface, were spot-welded to 0.02 in. 316 stainless shim stock, which then was welded to 3/16-inch, square cross-section 316 stainless steel ribs. In order to fit through HBT-EP's 8 in. vacuum ports, the segments were designed as a wide panel that would fit over the feedback sensors, and a narrow panel to fill the remaining space on the solid portion of the shell (Fig. 3).

The shim stock provided a good spot-welding surface that was made relatively conformal to HBT-EP's existing 316 stainless shells, and the frames provided (i) strength against the significant magnetic forces felt by a high-μ material in HBT-EP's toroidal field, and (ii) a means of mounting to the plasma-facing side of the existing shells. Although a single spot-weld was found to have sufficient strength to support the forces on an individual tile, each tile was double spot-welded to the shim stock to ensure against the possibility of a single bad weld.

The design of tiles spot-welded to shim stock on a steel frame also permitted us to design around the individual features of the HBT-EP shells. Each shell has a slightly off-nominal curvature, mostly bowing out but occasionally bowing in at the center of the poloidal arc. Although the nominal shell is at a minor radius of 16 cm at every point along its 90° curve, the as-built shells vary from 15.5 cm to almost 17 cm, meaning the design had to be flexible enough to fit a considerable range of curvatures. As a result, the ferritic wall panels stand off the stainless shells by as much as 1 cm in some places. The poloidal arc-length of the shells also vary by several millimeters, necessitating customization of the mounting frame to each shell.

Because the ferritic wall projects radially inward from the stainless shells, at maximum insertion, the ferritic wall can function as a plasma limiter. Including a retraction limit for

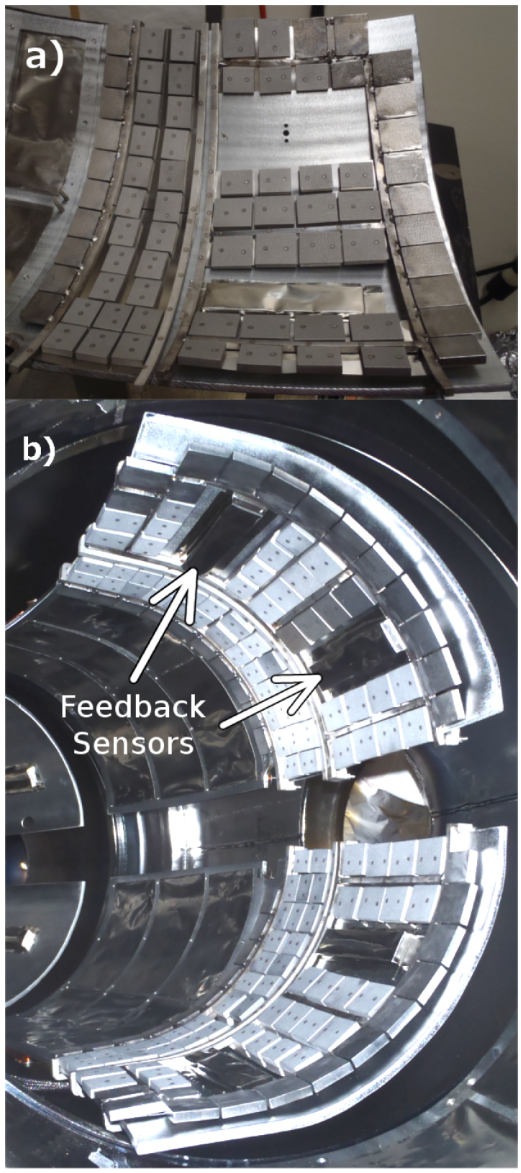

FIG. 3. Photographs of the ferritic wall inserts during installation. (a) Wall mounted to a spare shell on a workbench, showing wide and narrow wall panel designs. (b) Wall inserts installed on shells in-vessel, showing separation between shell and ferritic tiles, as well as feedback sensors (two per shell) in gaps between tiles. Appearance of tiles varies due to a change in the cleaning procedure to include sand-blasting after tumbling.

chamber safety, this permits a maximum range of plasma-wall separation from 5% to 23% of the plasma minor radius for the ferritic wall, as compared with 7%–33% for the unmodified stainless shells.

III. INSTALLATION

Due to the small variations in curvature and customized cut-outs between shells, each frame was first test-installed in order to allow customization to a particular shell. Each poloidal rib was designed with a U-hook to grab the top poloidal edge of the shell, and excess length at the other end. The frame was hooked onto the shell, and the poloidal ribs of each frame were marked with a stylus where the ribs met the midplane shell edge. A standard #8-32 stud was welded onto the outward face of the rib just below the mark, and the ribs were then trimmed of their excess length to minimize interference with shell insertion.

The panel was then cleaned thoroughly in acetone and methanol and re-installed, with custom L-brackets on the studs to grip the midplane shell edge, and set-screws fit into threaded holes in the U-hook to grip against the back of the shell. During the mid-point and end of installation, the toroidal field magnets were pulsed at full strength to ensure all ferritic wall segments were secure on their shells.

IV. TEST RESULTS

The first test of the ferritic segments after installation was verification of the magnetic forces and resulting shell displacements that would be experienced in the strong toroidal field gradient. The exact applied field required to saturate a ferritic sample depends on the sample's stress and annealing histories and geometry, but even out of saturation, the force exceeds the weight force on the tile. Although the HBT-EP shells were the best mounting point for plasma-wall coupling and for adjusting configuration without breaching vacuum, it was uncertain how much force the shell mounting system could sustain over many pulses. The HBT-EP shells are mounted to 30 cm long, 1 in. diameter 316 stainless steel tubes by a mounting bracket with set screws tightened against an aluminum block, and it was necessary to test the shell's tolerances before full installation.

To evaluate these magnetic forces, a Honeywell FS01 piezoelectric force transducer was purchased and calibrated with a precision weight set. A sample tile of Hiperco 50 alloy was affixed to the surface of the transducer, and the transducer was mounted to the outside of HBT-EP's vacuum vessel at the outboard midplane with the tile facing away from the machine center; the field gradient therefore pointed from the tile to the transducer. When the toroidal field magnets were energized, the transducer measured a peak sustained magnetic force about 5 times the weight force of the tile (Fig. 4).

As the toroidal field is stronger inside the vacuum vessel due to the $1/R$ field gradient, the forces were expected to

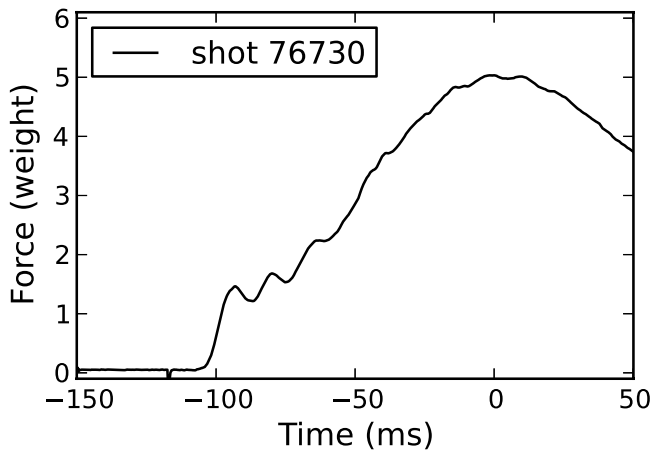

FIG. 4. Magnetic force measurements for a single tile outside the vacuum vessel at the outboard midplane, normalized to the tile's weight force. The toroidal field turns on at −117 ms and peaks near 0 ms.

be considerably stronger when mounted internally. Although significant, the forces, totaling several kilograms for enough material to cover the solid half of a shell, were considered small enough that it was safe to build and install a prototype ferritic wall insert to verify that installation could be accomplished quickly, identify any unexpected challenges, and quantify the effect of the magnetic forces on the shells in terms of shell deflection.

To measure the amount of shell deflection, a digital camera with 30 fps video recording capability was mounted to the machine, focused on a toroidal edge of the shell housing the prototype wall panels. Since the toroidal field pulse has a rise time of 117 ms, 30 fps was sufficient to capture a clear maximum-field frame. Selecting a reference frame from before the toroidal field pulse, an edge-finding algorithm was applied to both frames to measure radial and vertical shell deflections to ±0.15 mm or better precision. Under the highest setting of the toroidal field magnets, the edge of the shell was found to deflect by less than 2.5 mm, or less than 0.5° of angle around the shell armature. This was deemed to be an acceptable mechanical strain for long-term operation as it was comparable to the quantity of shell deflection observed while manually handling the shells during wall installation and prior in-vessel work. As a result, the maximum retraction limit of the ferritic shells was reduced by 5 mm to ensure shell motion would not damage the chamber.

Installation of the assembled ferritic wall segments on five of HBT-EP's ten shell pairs was accomplished in under one week. One shell pair does not include the narrow panels due to obstruction by a poloidal sensor array. Despite the significant amount of material installed in-vessel, due to careful observation of clean handling and vacuum preparation procedures, the time to return to 10 nTorr base pressure was similar to pump-down times following other substantial up-to-air operations.

Following a brief helium glow discharge cleaning and a typical series of deuterium clean-up plasmas to sputter adsorbed impurities from the walls, soft x-ray diagnostics showed little difference from plasma shots prior to the installation. This suggests the installation caused no significant changes in metal impurities.

One of the major concerns surrounding the installation of ferritic material close to the plasma boundary is that it might interfere with normal machine operation, particularly during plasma breakdown, either by distorting equilibrium fields or increasing vacuum contamination. Prior to installation, the control coils of every second toroidal section were energized (a $n = 5$, $m = 0$ perturbation) during breakdown to simulate the effect of the ferritic wall on the toroidal field, and no significant effects on plasma formation were observed. Following installation, HBT-EP returned to a very high vacuum with about the same pump-down time as past up-to-air operations, and has been able to operate normally since, using similar discharge programming and yielding plasmas with similar parameters to those seen before the ferritic wall upgrade.

Although general machine operation and performance has not changed significantly, as anticipated, the two feedback sensors on each upgraded shell are affected by their poloidal proximity to the ferritic material. Although the poloidal feedback sensors on shells with ferritic segments showed higher readings of vertical field pickup than their counterparts on unmodified shells by about 20% (Fig. 5) at typical equilibrium field settings, none of the other magnetic sensors indicated any significant poloidal or radial field perturbation by the ferritic upgrade, including the toroidal array and the two poloidal arrays (one of which is mounted to an upgraded shell). Therefore, these sensors can still be used to study MHD without needing to correct for effects from the ferritic wall.[13]

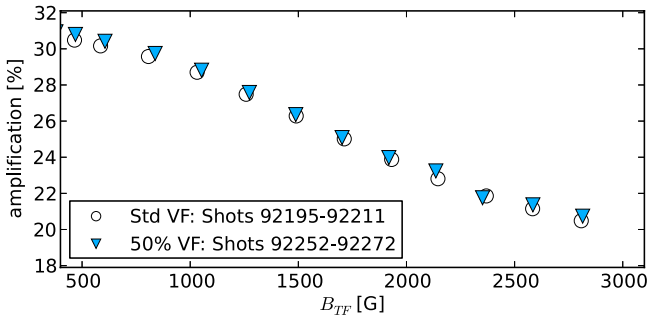

FIG. 5. Poloidal pickup from vertical field seen to be amplified on ferritic shells, relative to unmodified stainless shells. Lack of dependence on vertical field strength demonstrates fixed μ_r seen by poloidal fields, whereas dependence on B_{TF} indicates magnetic saturation. Variation between vertical field sets is within shot-to-shot variation.

V. VERIFICATION OF MAGNETIC PROPERTIES

In order to demonstrate that the ferritic wall is magnetically saturated, an experiment was conducted in which the toroidal and vertical field magnets were energized at a range of settings and observed on the midplane feedback sensors. In this experiment, changes in the wall's permeability were detected by measuring the changes in the ratio of the vertical field observed near the ferritic wall to that detected by equivalent sensors on unmodified, non-ferritic shells. Fig. 5 shows the results of these measurements as the toroidal field measured at the outboard midplane was changed from 500 G to 2.8 kG, at vertical fields of 50 and 100 G.

Because the amplification is independent of vertical field, the wall can be described as having a fixed value of μ_r as seen by the perturbed (poloidal) fields of surface instabilities, for a given value of toroidal field. The decrease of the amplification effect with increasing toroidal field strength indicates that the material must be magnetically saturated. In contrast, if the ferritic wall was unsaturated, both μ_r and the measured vertical field amplification would be effectively independent from the applied field. When saturated, $\mu_r \approx 1 + B_{sat}/B_T$, and the vertical field amplification should decrease with increasing B_T. In the experiment, as the applied toroidal field increased, the amplification of the vertical field decreased from 30% to 20% on ferritic shells compared to nonferritic shells, corresponding to the gradual decrease of relative permeability. Since the saturation induction B_{sat} of Hiperco 50 is 2.4 T (24 kG) as noted in Section II, at a local toroidal field B_T of 2.8 kG, this indicates $\mu_r \approx 9$ at the low-field midplane. Averaging over the arc of the ferritic wall gives an average $\mu_r \approx 8$, within the target range.

VI. OBSERVATION OF FERRITIC WALL EFFECTS

HBT-EP's movable ferritic walls have allowed controlled experiments and observations of plasma stability as plasma-wall separation was varied between 9% and 23% of the plasma's minor radius, spanning the reactor geometry regime. Preliminary experiments using the new ferritic wall have shown an increased plasma response to applied resonant magnetic perturbations, enhanced vulnerability to disruptions, and increased growth rates for kink instabilities when the ferritic wall is positioned close to the plasma surface.[13] These initial results demonstrate the importance of including the effects of saturated, close-fitting ferritic materials in the design and operation of tokamaks at high performance and near stability limits.

ACKNOWLEDGMENTS

The authors wish to thank J. Andrello, T. M. Roberts, and Huade Tan for technical support, and W. Bailey for assistance in the characterization of magnetic materials. This work was supported by the U.S. Department of Energy Grant No. DE-FG02-86ER53222.

[1]A. Kohyama, A. Hishinuma, D. S. Gelles, R. L. Klueh, W. Dietz, and K. Ehrlich, J. Nucl. Mater. **233-237**, 138 (1996).
[2]Steven J. Zinkel, Phys. Plasmas **12**, 058101 (2005).
[3]K. Tsuzuki *et al.*, Nucl. Fusion **46**(11), 966 (2006).
[4]G. Kurita, T. Tuda, M. Azumi, S. Ishida, S. Takeji, A. Sakasai, M. Matsukawa, T. Ozeki, and M. Kikuchi, Nucl. Fusion **43**, 949 (2003).
[5]V. D. Pustovitov, Phys. Plasmas **16**, 052503 (2009).
[6]W. F. Bergerson, D. A. Hannum, C. C. Hegna, R. D. Kendrick, J. S. Sarff, and C. B. Forest, Phys. Rev. Lett. **101**, 235005 (2008).
[7]D. A. Maurer *et al.*, Plasma Phys. Controlled Fusion **53**(7), 074016 (2011).
[8]A. Kohyama, A. Hishinuma, Y. Kohno, K. Shiba, and A. Sagara, Fusion Eng. Des. **41**, 1 (1998).
[9]M. Enoeda *et al.*, Fusion Eng. Des. **87**, 1363 (2012).
[10]Carpenter Technology Corporation (2006), http://www.cartech.com/techarticles.aspx?id=1476.
[11]Carpenter Technology Corporation (1990), http://cartech.ides.com/datasheet.aspx?i=103&e=200&c=TechArt.
[12]T. Miyazaki and H. Jin, *The Physics of Ferromagnetism* (Springer, 2012).
[13]J. P. Levesque, P. E. Hughes, J. Bialek, P. J. Byrne, M. E. Mauel, G. A. Navratil, Q. Peng, D. J. Rhodes, and C. C. Stoafer, Phys. Plasmas **22**, 056102 (2015).